Structural, Microstructural and Electrical Properties of Lanthanum (La^{+3})-Modified Lead Iron Niobate $Pb(Fe_{0.5}Nb_{0.5})O_3$

Thesis submitted for the award of degree

Master of Science

in

Physics

by

Soumya Ranjan Dash

(Roll No: 410PH2125)

Under the academic autonomy

National Institute of Technology, Rourkela

Under the supervision of

Dr. Dillip Kumar Pradhan

Department of Physics

National Institute of Technology

Rourkela-769008, Odisha, India

May-2012

Department of Physics

National Institute of Technology, Rourkela

Rourkela-769008, Orissa, India

CERTIFICATE

This is to certify that the thesis entitled **"Structural, Microstructural and Electrical Properties of Lanthanum (La^{+3})-Modified Lead Iron Niobate $Pb(Fe_{0.5}Nb_{0.5})O_3$"**, submitted by **Soumya Ranjan Dash** to National Institute of Technology, Rourkela, is a record of bonafide research work under my supervision and I consider it worthy of consideration for the award of the degree of Master of Science of the Institute.

Date:

Dr. Dillip Kumar Pradhan

Asst. Professor
Department of Physics
National Institute of Technology
Rourkela, 769008

DECLARATION

I hereby declare that the work carried out in this thesis is entirely original. It was carried out by me along with Miss Shreenu Pattanaik at Department of Physics, National Institute of Technology, Rourkela. I further declare that it has not formed the basis for the award of any degree, diploma, or similar title of any university or institution.

Soumya Ranjan Dash

Roll No- 410PH2125

Department of physics

National Institute of Technology

Rourkela-769008

ACKNOWLEDGEMENT

I avail this opportunity to express my deep sense of gratitude to my supervisor **Dr. Dillip Kumar Pradhan**, **Dept. of Physics, NIT, Rourkela** for his invaluable guidance, motivation, untiring efforts and meticulous attention at all stages during my course of work.

I express my sincere thanks to **Prof. Siddharth Jena, Head of the Department of Physics and the faculty members, NIT, Rourkela** for providing me the necessary facilities in the department.

I express my profound gratitude to **Mr. Satya Narayana Tripathy, Research scholar, Departmentof Physics**, for his ceaseless encouragement, valuable suggestions and constant help forthis work.

I am thankful **Sri U.K. Sahu, technical assistant (XRD), Metallurgical & Materials Engineering**, for his co-operation in experimental work.

Special thanks to my friends **Abakash, Bamadev, Dipti, Paradarsini, Pratap, Ramesh, Sanjaya, Srikanta, Surya bhai,** department of Physics and Chemistry for being so supportive and helpful in every possible way.

Last but not the least I would like to thank my sister **Shreenu Pattanaik**, NIT, Rourkela with whom I have completed a part of this project work. Her cooperation during this tenure is highly acknowledged. Lastly I sincerely thank to all those who have directly or indirectly helped for the work reported here in.

Above all I am grateful to parents, brother and sisters, for the tremendous amount of inspiration and moral support they have given me since my childhood.

Date: **Soumya Ranjan Dash**

Place: (410PH2125)

Dept. of physics
NIT, Rourkela

Contents

Abstract

Lanthanum-modified Lead iron niobate ceramic oxides having chemical formula $Pb_{(1-x)}La_x(Fe_{0.5}Nb_{0.5})_{(1-x/4)}O_3$ (x=0.00, 0.02, 0.04, 0.06, 0.08) have been prepared using traditional solid state reaction route. Preliminary structural, microstructural and electrical studies were carried out by the powder x-ray diffraction, scanning electron microscopy and complex impedance spectroscopic technique in awide experimental conditions. The x-ray diffraction study confirmed the formation of perovskite structures of the newly modified ceramics. The lattice parameters were calculated using standard IUCR software CHECKCELL. Crystallite sizes of the samples were calculated from Williamson-Hall method. Microstructure/morphology of the materials was analyzed from SEM images. Dieletric and impedance spectroscopic studies of the materials were carried out as a function of temperature for a wide range of frequencies. The pure PFN ceramic oxide shows the phase transition from ferroelectric to paraelectric state around 115^0C. There is a notable decrease in the transition temperature of La-PFN(x=0.02) ceramic and above 4% La concentration, the transition temperature falls below room temperature.

CHAPTER 1

1.1 Introduction

Significant advances have been made in the field of ferroelectrics due to its fundamental physical and potential device applications. The phenomenon of ferroelectricity was discovered in 1921 by Valsek in Rockchell salt **[1]**. Since the discovery of barium titanate ($BaTiO_3$), breakthrough in the research on ferroelectric materials came in picture during 1950's, leading to the widespread use of lead based ceramics in capacitor applications and piezoelectric transducer device applications. Since then, many other ferroelectric ceramics including lead titanate ($PbTiO_3$), lead zirconate titanate (PZT), lead lanthanum zirconate titanate (PLZT), and relaxor ferroelectrics like lead magnesium niobate (PMN) have been discovered, studied and utilized for a variety of potential device applications **[2]**. With the development of advanced ceramic processing and thin film technology, many new device applications have emerged. The largest application of ferroelectric ceramics has been in the areas such as dielectric ceramics for capacitor application, ferroelectric thin film for non-volatile memories, piezoelectric materials.

Ceramics are defined as compounds that consist of metallic and non-metallic elements which are synthesized by the application of temperature and pressure. The properties of the ceramics are wear-resistant, brittle, refractory, thermal insulators, electrical insulators, nonmagnetic, oxidation resistance, and thermal shock prone and chemically stable. The property of the ceramic materials is represented by nature of bonding between the atoms and type of atoms. Ceramic materials are basically covalent and ionic bonded **[3].**

Most of the ceramic materials are dielectrics which can be controlled by electrostatic field. Electrical conductivity of ceramics basically depends on temperature and frequency. This is due to the reason that charge transport mechanisms are frequency and temperature dependent. Thermal energy provides the activation energy for the charge migration. In general, ceramic materials have high dielectric strength for storage device applications.

1.1.1 Characteristics feature of the ferroelectric materials

(1) Lack of center of symmetry i.e. spontaneous polarization.

(2) Ferroelectric crystals must be piezoelectric though the converse is not true.

(3) Ferroelectric materials have one or more Curie temperature.

(4) Ferroelectric transitions are structural transitions.

(5) Ferroelectric materials obey Curie-Weiss law.

(6) Ferroelectric materials exhibits hysteresis loop.

The ferroelectrics are characterized by the ferroelectric hysteresis loop, i.e., the polarization is a double-valued function of the applied electric field. As the electric field is high enough, all the ferroelectric domains are aligned in the direction of field, and the polarization is saturated. The extrapolation of the linear portion of the curve at high field back to the polarization axis represents the value of the spontaneous polarization P_s. When the electric field is removed, most of the domains remain aligned and the crystal still exhibit polarization **[4]**. The polarization at zero fields after saturation is called remnant polarization P_r. The remnant polarization can be removed when a field in the opposite direction is applied and reaches a critical value. The

strength of the electric field required to reduce the polarization to zero is called the coercive field E_c.

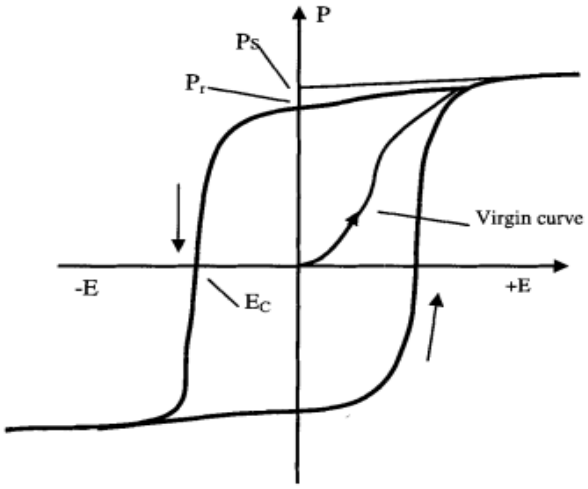

(Fig 1.1.1: Typical hysteresis loop of ferroelectric material)

1.1.2 Division of ferroelectric materials

- Corner Sharing Octahedra
    - (1) Perovskites (ABO_3)
    - (2) Pyrochloro ($A_2B_2O_7$)
    - (3) Tungsten Bronze type Compounds ($(A_1)_2(A_2)_4(C)_4(B_1)_2(B_2)_8O_{30}$)
    - (4) Bismuth Oxide Layer Structured Ferroelectrics $((Bi_2O_2)^{+2}, (A_{n-1},B_n\ O_{3n-1})^{-2})$
- compounds containing hydrogen bonded radicals
- organic polymers
- ceramic polymer composites

1.2 Perovskite structure:

Among different ferroelectrics perovskites are most studied materials for device applications.

The perovskite structure, of chemical formula ABX_3, consists of two distinct cation sites (A and B) and one anion site (C). Crystals of the prototypical perovskite, $CaTiO_3$, were first discovered in 1839. A-site can be monovalent, divalent or trivalent and B-site can be pentavalant, tetravalent or trivalent .The coordination number of A-site cation is 8 to 10 and B-site cation is 6.

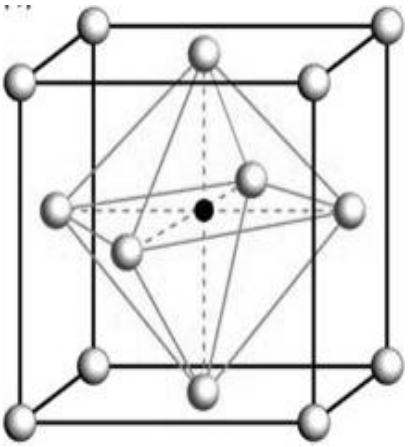

(Fig 1.2: Perovskite Structure (ABO_3)

The structures of perovskites are determined by short range attractive (bonding) and repulsive forces between nearby ions, as well as long range electrostatic interactions between unit cells. The stability of perovskite is represented by tolerance factor (t) and determines the property of the perovskite.

$$t = \frac{(R_A + R_O)}{\sqrt{2}(R_B + R_O)}$$

(1) $t \geq 1$, for ferroelectric perovskites, $BaTiO_3$, $PbTiO_3$ and $KNbO_3$,

(2) $t < 1$ for antiferroelectric perovskites $PbZrO_3$, $NaNbO_3$ and $BiFeO_3$.

(3) $t=1$ corresponds to an ideal perovskite

While at $t<1$ Indicates tilting or rotation of the BO_6 octahedral and for $t>1$ a displacive distortion within the BO_6 octahedral.

1.3 Ferroelectric Phase Transition

The transition from ferroelectric (non-centro symmetric) to paraeletric (centro-symmetric) phase is accompanied by a structural or crystallographic phase transition. In phase transition quite often referred to symmetry breaking.

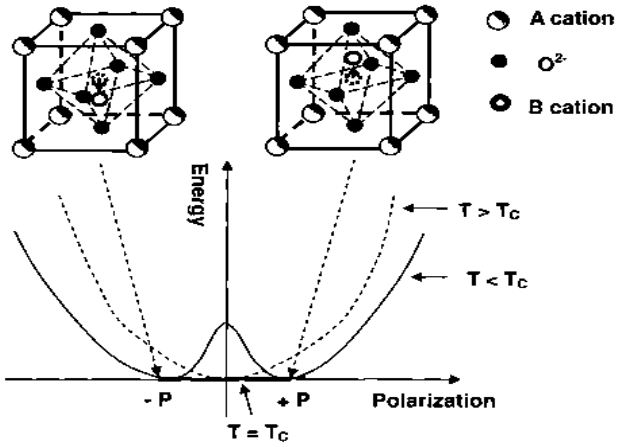

Fig 1.3: B cation off-centre displacement and the double-well energy diagram of ABO_3 ferroelectrics

Types of ferroelectric phase transition

(1) Displacive phase transition

(2) Order-disorder phase transition

Displacive transitions proceed through a small distortion of the bonds (dilatational or rotational). As the key for the ferroelectricity, spontaneous polarization arises due to the non-coincidence of the positive and negative charge centers in the unit cell that implies non-centrosymmetric nature. In ABO_3 ferroelectricity results from the off center displacement of the B cation leading to displacive phase transition **[5]**. This off center displacement in the perovskite ferroelectrics is the

result of competition between the short range repulsion force between adjacent electron clouds of ions, which favors the non-ferroelectric centro-symmetric structure and additional bonding between B cation and oxygen ions.

Order-disorder transitions proceed through substitution between atoms possibly followed by small atomic displacements. They are commonly found in metals and alloys but also in some ceramics.

1.4 Order Parameter

The phase transitions are characterized by the appearance of some non-zero quantity in the ordered state and the same vanishes in the disorder state. Such quantity is called order parameter. Type of phase transition according to order parameter.

(1) First order phase transition, characterized by the appearances of latent heat, finite change in volume and hysteresis. (First derivative of Gibb's free energy is discontinuous.)

(2) A second order phase transition, characterized by discontinuity in the specific heat. (Second derivative of Gibb's free energy is discontinuous.)

It is known that order parameter is a decreasing function of temperature and must varnish at critical temperature. If the order parameter vanishes discontinuously at T_c, then the transition is said to be first order while if it vanished continuously, it is called second order. Near the Curie point or phase transition temperature, thermodynamic properties including dielectric, elastic, optical, and thermal constants show an anomalous behavior. This is due to the distortion in the crystal as the phase changes. The temperature dependence of the dielectric constant above the Curie point ($T>T_C$) in most of the ferroelectric crystals is governed by the

Curie-Weiss law:

$$\varepsilon = \varepsilon_0 + \frac{C}{T - T_0}$$

Where, ε is the permittivity of the material, ε_0 is the permittivity of the vacuum, C is the Curie constant and T_0 is the Curie-Weiss temperature. In general the Curie-Weiss temperature T_0, is different from the Curie temperature T_C. For first order transitions, $T_0 < T_C$ while for second order phase transitions, $T_0 = T_C$.

Complex perovskite type ferroelectrics basically show DPT (diffuse phase transition) which is characterized by a broad maximum for the temperature dependence of dielectric constant (ε) and dielectric dispersion in the transition region. For DPT, ε follows modified temperature dependence Curie Weiss law.

$$\varepsilon = \varepsilon_0 + \frac{C}{(T - T_m)^{\upsilon}}$$

where, T m is the temperature at which ε reaches maximum (ε_m), C is the modified Curie constant and γ is the critical exponent. The γ factor explains the diffusivity of the materials, which lies in the range $1<\gamma<2$. In case of γ equals to unity, normal Curie–Weiss law is followed and it shows the normal ferroelectric phase transition.

CHAPTER 2

Literature Survey

2.1 Lead Iron Niobate and related materials

Lead iron niobate Pb ($Fe_{0.5}$ $Nb_{0.5}$) O_3 (PFN) is a lead based complex perovskite which is of great interest for multilayer capacitors owing to its high dielectric constant discovered by Smolenskii *et al* **[6]**. PFN exhibits monoclinic structure with a Curie temperature of 114 °C, therefore becomes a possible candidate for making new relaxor ferroelectrics exhibiting attractive piezoelectric properties. It has been studied ceramic powders, single crystal and also thin films. Raymond *et al* **[7]**. extensively studied the structural, thermoelectric, dieletric and impedance spectroscopic studies of lead iron niobate. Wang *et al* **[8]**. showed the enhanced dielectric properties in 0.94PFN-0.06PT single crystals. Kumar *et al* **[9]**. studied the enhanced electrical properties of PFN thin films. Mishra *et al* **[10]**. reported the dieletric relaxation and magnetic properties of the PFN ceramics. Sahoo *et al* **[11]**. studied the effect of $V5^{+}$ and Y^{+3} substitutions on dieletric and ferroelectric properties of PFN. Varshney *et al.* reported the dieletric properties of Ba^{2+} modified lead iron niobate.

2.1.1 Based on the literature survey, some of the main problems associated with PFN based material are

(1) Difficult to synthesize single phase PFN material. For example, when synthesized using conventional solid-state synthesis route, a pyrochloro phase ($Pb_3Nb_4O_{13}$ or $Pb_2Nb_2O_7$ type) with lower dielectric constant always coexists with the desired perovskite phase in PFN ceramics.

(2) PFN ceramics or similar iron-doped systems, the occurrence of Fe^{2+} and oxygen vacancies originated during the sintering process increase electrical conductivity, large frequency dispersion of dielectric constants, dielectric loss, space-charge accumulation at the grain boundary, all of them inhibition to optimal device performance. PFN ceramics also exhibit lower resistivity, for example, makes it almost impossible to pole PFN ceramics to determine the piezoelectric constants as well as to measure the polarization hysteresis characteristics.

Among the various methodologies available in literature, one of the important methods to solve the above mention problems is suitable substitutions. In the present study, we have planned to substitute La at the Pb-site of the complex perovskite PFN.

2.2 Materials under investigation:

$$Pb_{(1-x)}\ La_{x}\ (Fe_{0.5}\ Nb_{0.}5)_{1-x/4}\ O_3$$

(x=0.00, 0.02, 0.04, 0.06, 0.08)

2.3 Main Objectives:

The following will be the main objectives of the proposed work.

(1) Preparation of La modified PFN compounds using high temperature solid state reaction route.

(2) Studies of the structural & micro-structural properties of the materials.

(3) Studies of dielectric responses as a function of frequency & temperature.

(4) Studies of Impedance and conductivity studies of the sample.

CHAPTER 3

Experimental Technique

This chapter discuss about the basic principles and various analytical techniques used for the preparation as well as characterization of ceramic materials. After preparation of the studied material, they have been subjected to a series of tests that include structural analysis, surface morphology study and dielectric measurements.

3.1 Introduction

Many of the important aspects of present-day ceramic fabrications are required to produce, a material with specific properties, a body of required shape and size within specified dimensional tolerances and the required component at an economic cost **[13]**. Eventually synthesis of these materials is of a greater importance to the progress of material science. The fabrication process comprises five stages: the specification, purchase and storage of raw materials; preparation of a composite in powder form; forming the powder into a shape; densification; finishing. There are several method for synthesis of ceramic materials such as solid state reaction route, high energy ball milling (top to bottom approach), soft chemical route (bottom to top approach). To achieve a qualitative product with respect to purity, homogeneity, reactivity each method is having its own advantages and disadvantages. In this view, solid-state reaction route is found to be easier and low cost method by means of performance and economy.

3.2 Solid State reaction route

The solid state reaction route is one of the commonly used method for breaking up of agglomerates and forming an intimate mixture of constituents in order to prepare polycrystalline ceramics from a mixture of starting raw materials. Mixing of solids do not take place at room temperature over normal time scales, so it is necessary to heat them to much higher temperatures. The various factors which affect the feasibility and rate of a solid state reaction are, reaction conditions, structural properties of the reactants, surface area of the solids, their reactivity and the thermodynamic free energy change associated with the solids. In addition, the higher temperature allows the interdiffusion of neighbouring particles which increases the probability of formation of desired compound and the time taken to complete the process will be proportional to the square of the particle size. If the particles are consisting of aggregates of crystals rather than individual crystals then the whole process will be considerably slower **[14]**. A number of procedures are used to reduce the time needed for synthesis. Chemical composition, particle size, degree of aggregation and reactivity are few important aspects that specify the choice of raw material in order to carry out the solid state reaction process.

3.3 Experimental Details

Polycrystalline powder of $Pb_{(1-x)}La_x(Fe_{0.5}Nb_{0.5})_{1-x/4}O_3$ (x=0.00, 0.02, 0.04, 0.06, 0.08) were synthesized by a conventional solid-state reaction route.

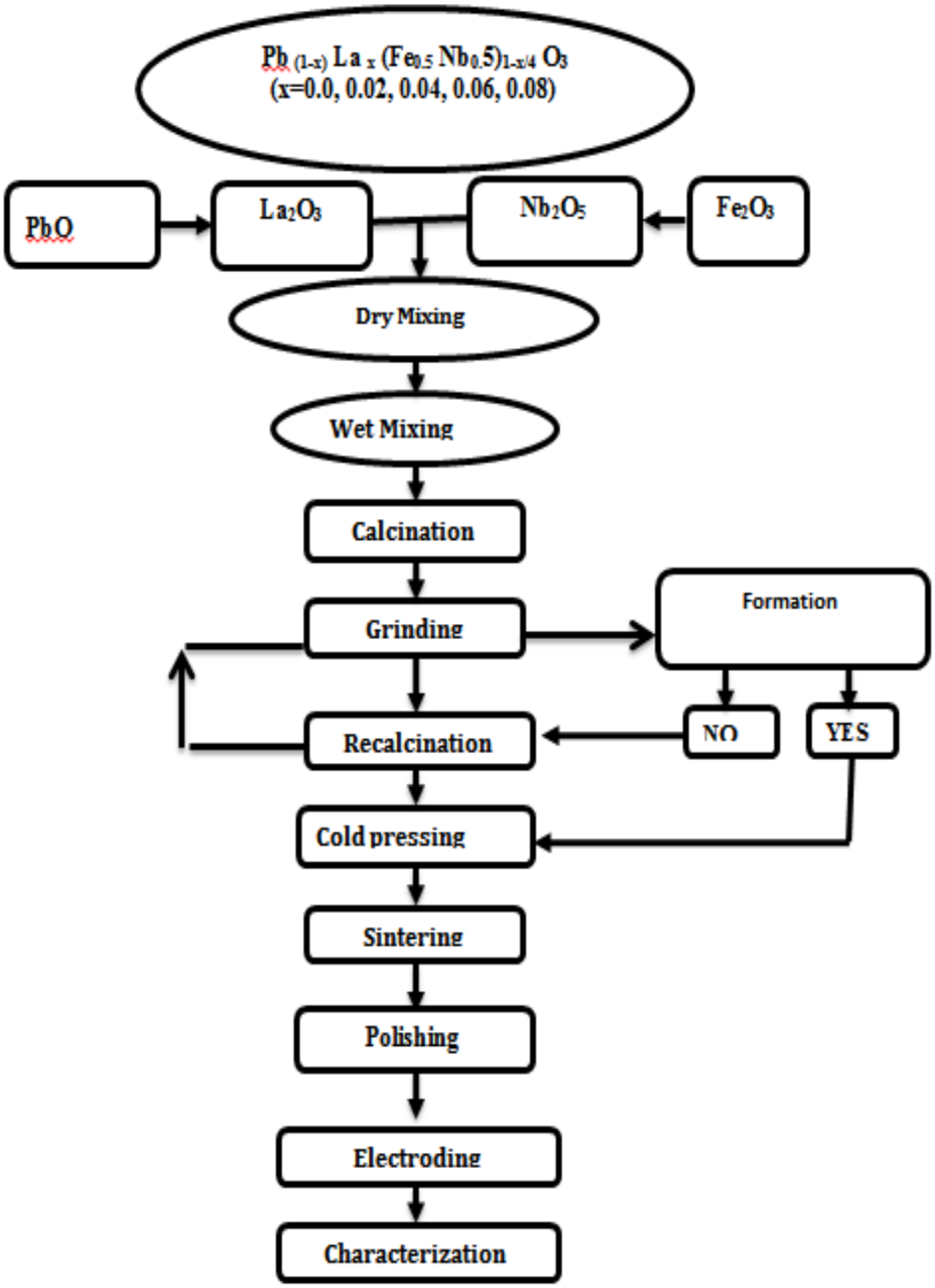

Fig 3.3: Flow chart for the preparation of samples by a solid-state reaction technique.

The high purity oxides (PbO, Fe_2O_3, Nb_2O_5, La_2O_3,) (LOBA Chemie Private Limited, Mumbai, India) of required precursors were weighed according to the stoichiometric ratios and mixed by agate mortar and pestle for 2 hours then in wet (acetone) medium to obtain a homogeneous mixture for 4 hrs. As the melting point of lead (II) oxide is 888^0C which is less than the calcined temperature, so 3% extra PbO was taken in order to compensate lead loss at high temperature. The dried mixture was put in alumina crucible and calcined at a particular temperature about 900 ^{O} C for 6 hours in furnace. The above calcined powder formed into a lump as it had usually undergone a limited amount of sintering and it was grinded till it becomes fine powder. Phase formation was checked by XRD at room temperature. The above calcined powder was incorporated with an organic binder of 6% PVA (polyvinyl alcohol) in mortar and pestle. The primary function of the binder was to give a dry shape of sufficient strength to survive the handling necessary between shaping and sintering. The binder mixed powder was compacted to form pallet by a hydraulic press at 6 x 10^{7} kg/m^{2} pressure using 10mm die set. The sintering of the pellet sample was carried out at an optimized temperature of 1000 ^{O}C. The sintered pallets were polished by emery paper and painted with silver paste as an electrode for electrical measurement.

3.4 X-ray powder diffraction

X-ray diffraction is a (XRD) powerful non-contact and non-destructive technique, which makes it ideal for situ studies. It uniquely identifies the crystalline phases present in the material and measures the structural properties like phase composition, grain size, preferred orientation, strain state, defect structure and epitaxy of these phases present in the compound. The intensities obtained from the XRD can provide quantitative as well as accurate information on the atomic arrangements at interfaces. Materials having different composition of elements can be

successfully identified with XRD, but it are very much sensitive to the elements having large atomic number, because the diffracted intensities are very large as compared to the elements having lower atomic number. It predicts the quantitative phase analysis as well as qualitative structural and microstructural analysis. The wavelength λ of X-ray beam is typically 0.7 - 2 Å which corresponds to X-ray energies (E = 12.4 keV / λ) of 6 – 17 keV. X-rays are used to produce the diffraction pattern because their wavelength is typically the same order of magnitude (1–100 angstroms) as the spacing *d* between planes in the crystal.

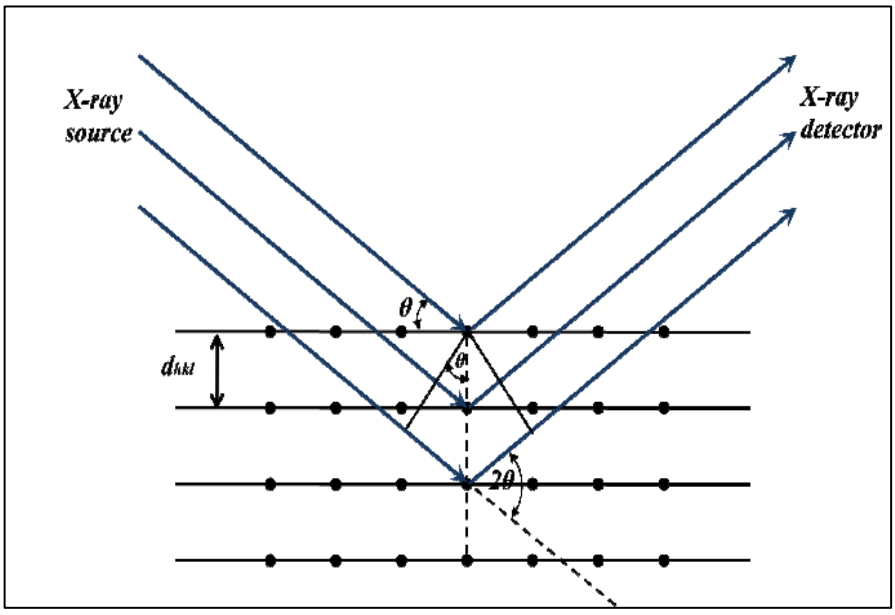

Fig 3.4: Demonstration of Bragg's law

The diffraction satisfies the Bragg equation

$$2d\sin\theta = n\lambda$$

Here *d* is the spacing between diffracting planes, θ is the incident angle, *n* is any integer, and λ is the wavelength of the beam.

The information in an XRD pattern is a direct result of three things:

1. The size and shape of the unit cells, which determine the relative positions of the diffraction peaks.

2. Atomic positions within the unit cell, which determine the relative intensities of the diffraction peaks electron (charge density distribution)

3. Peak broadening is related to microstructural parameters (crystallite size, r.m.s strain and dislocation density)

It is impossible to find two different materials having same x-ray diffraction pattern. Therefore it can be used as *fingerprint* to identify the material.

The determination of lattice constants from the line positions or d spacing can be found from a general formula

$$\frac{1}{d_{hkl}^2} = V^2[h^2b^2c^2\sin^2\alpha + k^2c^2a^2\sin^2\beta + l^2a^2b^2\sin^2\gamma]$$

Where; V = volume of the unit cell

$$= abc(1 - \cos^2\alpha - \cos^2\beta - \cos^2\gamma + \cos\alpha\cos\beta\cos\gamma)^{1/2}$$

Here **a, b, c, α, β** and **γ** are lattice parameters and **h, k, l** are the miller indices. The above formula is used to calculate lattice parameters for all the compositions **[15].**

The microstructural parameters crystallite size (**D**) and strain are related by Williamson-Hall Equation.

$$\beta \cos\theta = 4\epsilon \sin\theta + \lambda/D$$

Here β is full width half maxima and **Є** is the r.m.s strain in the material.

In the present study we have recorded the XRD-pattern using PAnalytic diffractometer.

3.5 Scanning electron microscopy

The scanning electron microscopy (SEM) is a powerful non-destructive imaging technique that scans the surface of specimen to study the topography, morphology and composition of the materials with much higher resolution. When a highly energetic electron beam strikes the specimen, ejection of the secondary electrons (SE), x-rays and back-scattered electrons (BSE) takes place from the sample surface. These electrons are then collected by the detector and convert into signal that displays on a screen. The magnification in a SEM can be varied from 10X -300,000X. In the present study, the SEM micrograph was taken on the scanning electron microscope (JEOL-330 scanning microscope JEOL). As the samples are non-conducting, a thin layer of platinum is coated using a sputter coater.

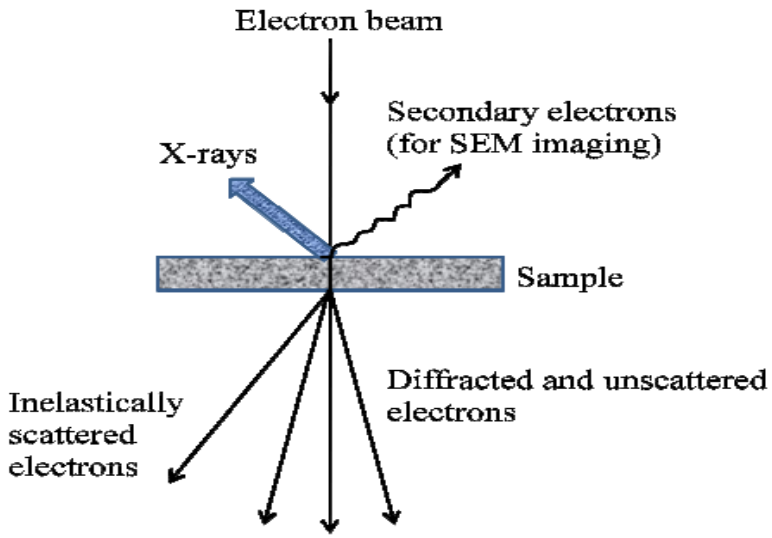

(Fig 3.5: Interaction of electron beam with specimen)

3.6 Dielectric Study

The dielectric study of a ceramic material gives valuable information about the behavior of localized electric charge carriers that leads to a greater understanding about the mechanism of dielectric polarization in the material. A good dielectric is, of course, necessarily a good insulator but the converse is not possible. When a dielectric material is subjected to an external electric field, the material becomes polarized due to induced dipole and permanent dipole moments. The polarization is directly proportional to the macroscopic field i.e.

$$\mathbf{P = \alpha E}$$

Here α is the polarizabilty of atoms and molecules**.**

Types of polarizations are

1. Electronic polarization
2. Atomic or ionic polarization
3. Dipolar polarization
4. Interface or space charge polarization

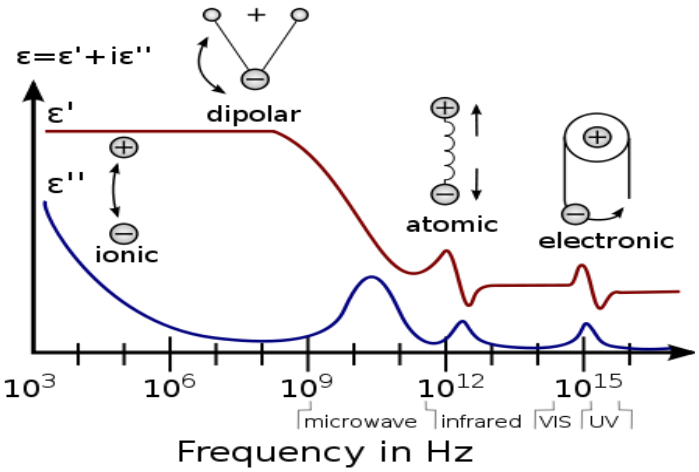

Fig 3.6: Frequency dependent dielectric constant

When a dielectric is subjected to the ac voltage, the electrical energy is absorbed by the material and is dissipated in the form of heat. The dissipation is called dielectric loss (tanδ). So for a dielectric material, the conductivity increases if dielectric loss increases. This relation can be written as:

$$\sigma_{a.c}=\omega\varepsilon''=\omega\varepsilon' \tan\delta$$

where $\varepsilon'' = \varepsilon' \tan\delta$

A.c. conductivity is one of the studies that give correlation between microstructure and electrical properties of the material. This technique is generally applied on the solids in order to characterize the bulk resistance of the material. In this work , to measure the relative permittivity (dielectric constant) and dielectric loss PSM 1735 was used .The electroded samples were used to make the measurements. The PSM was interfaced with the computer and the data (capacitance and D factor) was collected as a function of temperature at different frequencies. The measured capacitance was then converted into dielectric constant using the following formula:

$$\mathbf{C= \varepsilon_o \varepsilon_r A / d}$$

$$\mathbf{\varepsilon_r =C\ d/ \varepsilon_o A}$$

Where, C: Capacitance in farad (F)

ε: Permittivity of free space in farad per meter (8.85×10^{-12} F/m)

ε_r: Dielectric constant or relative permittivity of the sample.

A: Area of each plane electrode in square meters (m^2)

d: Separation between the electrodes in meters (m)

CHAPTER 4

Results and Discussion

4.1 Structural analysis

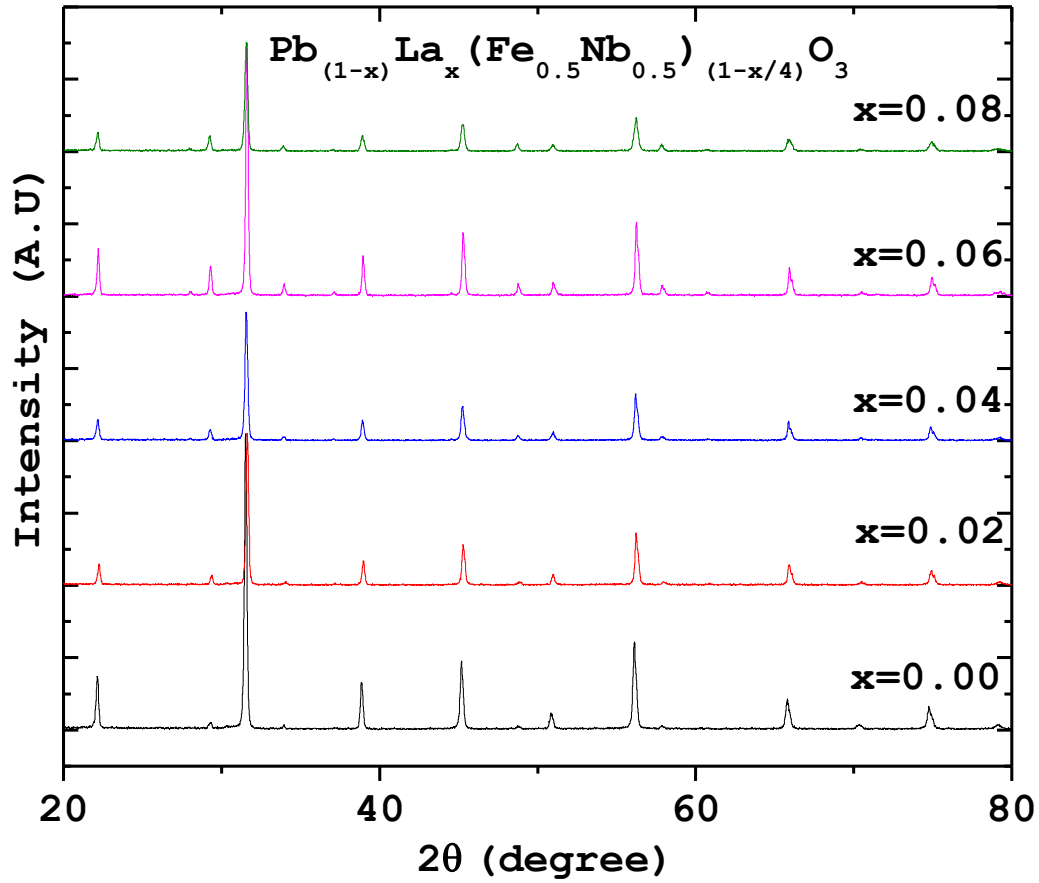

(Figure 4.1: Room temperature X-ray diffraction pattern of $Pb_{(1-x)}La_x(Fe_{0.5}Nb_{0.5})_{(1-x/4)}O_3$ (x=0.00,0.02,0.04,0.06,0.08))

Figure 4.1 represents the room temperature XRD patterns of calcined powder of $Pb_{(1-x)}\ La_x\ (Fe_{0.5}\ Nb_{0.5})_{(1-x/4)}O_3$ (x=0.00,0.02,0.04,0.06,0.08). The diffraction pattern is different from that of ingredients suggest the formation of PFN with a presence of small amount of pyrochloro phase (around the peak position of 27^o). It has also been observed that, with the increase in substitution concentration of Lanthanum (La^{+3}) there is a change in the peak position, peak intensity and peak shape of PFN. The full width at half maximum FWHM (β) and intensity of each peak were calculated using commercially available software (PEAK FIT). Indexing of X-ray diffraction patterns was carried out using the input parameters as diffraction angle (2θ) and intensity value of each peak by a standard open source IUCR software ***CHECK-CELL***. The best agreement in observed and calculated 2θ (i.e., $\Delta\theta$ ($2\theta_{obs}$-2_{cal}) = minimum) for monoclinic system (Table-4.1(a)). The crystal structure was found to be monoclinic for all compositions. The lattice parameters, unit cell volume, of the samples are listed (Table-4.1(f)).The lattice parameters were observed to be decrease with increase in La concentration. The decrease in the Peak intensity with increase in La^{+3} substitutions may be due to decrease in the crystallite size i.e. increasing in amorphous nature.

Table-4.1(a): (h, k, l) planes obtained for the composition x= 0.00

$Pb_{(1-x)}\ La_x\ (Fe_{0.5}\ Nb_{0.5})_{(1-x/4)}O_3$ x=0.00						
Sl No.	2θ(observed) degree	2θ(calculated) degree	2θ difference	h	k	l
1	22.1344	22.1357	-0.0013	0	0	1
2	31.5138	31.4979	0.0159	2	0	0
3	38.8482	38.8370	0.0112	0	2	1
4	45.1709	45.1561	0.0148	0	0	2
5	50.7530	50.8009	-0.0479	-1	1	2
6	56.1055	56.0951	0.0104	0	2	2
7	65.8126	65.8299	-0.0173	2	2	2
8	70.3305	70.3272	0.0033	0	0	3
9	74.7229	74.7076	0.0153	-1	1	3

Table 4.1(b): (h, k, l) planes obtained for the composition x= 0.02

$Pb_{(1-x)}$ La_x $(Fe_{0.5}$ $Nb_{0.5})_{(1-x/4)}O_3$ x=0.02						
Sl No.	2θ(observed) degree	2θ(calculated) degree	2θ difference	h	k	l
1	22.2348	22.1780	0.0568	-1	1	0
2	31.6164	31.5551	0.0613	0	2	0
3	38.9645	38.9607	0.0038	2	0	1
4	45.2759	45.2461	0.0298	-2	2	0
5	50.9582	50.9709	-0.0127	2	2	1
6	56.2217	56.1961	0.0256	1	3	1
7	65.9011	65.8863	0.0148	0	4	0
8	70.4006	70.4054	-0.0048	1	3	2
9	74.8287	74.9018	-0.0731	-2	4	0

Table 4.1(c): (h, k, l) planes obtained for the composition x= 0.04

$Pb_{(1-x)}$ La_x $(Fe_{0.5}$ $Nb_{0.5})_{(1-x/4)}O_3$ x=0.04						
Sl No.	2θ(observed) degree	2θ(calculated) degree	2θ difference	h	k	l
1	22.0875	22.1322	-0.0447	0	0	1
2	31.5523	31.5505	0.0018	0	2	0
3	38.7717	38.8164	-0.0447	-2	0	1
4	45.2336	45.2003	0.0333	-2	2	0
5	50.9489	50.9088	0.0401	2	2	1
6	56.1892	56.1764	0.0128	1	3	1
7	65.8144	65.8506	-0.0362	2	2	2
8	70.4006	70.4254	-0.0248	0	4	1
9	74.7496	74.7166	0.0330	-1	1	3

Table 4.1(d): (h, k, l) planes obtained for the composition x= 0.06

$Pb_{(1-x)}$ La_x $(Fe_{0.5}$ $Nb_{0.5})_{(1-x/4)}O_3$ x=0.06						
Sl No.	2θ(observed) degree	2θ(calculated) degree	2θ difference	h	k	l
1	22.1666	22.1807	-0.0141	-1	1	0
2	31.5940	31.5574	0.0366	0	2	0
3	38.8508	38.8773	-0.0265	0	2	1
4	45.2734	45.2519	0.0215	-2	2	0
5	50.8698	50.8452	0.0246	1	1	2
6	56.2343	56.1815	0.0528	1	3	1
7	65.8144	65.8374	-0.0230	2	2	2
8	70.4006	70.4371	-0.0365	0	4	1
9	74.9078	74.9162	-0.0084	3	3	1

Table 4.1(e): (h, k, l) planes obtained for the composition x= 0.08

$Pb_{(1-x)}\ La_x\ (Fe_{0.5}\ Nb_{\ 0.5})_{(1-x/4)}O_3$ x=0.08						
Sl No.	2θ(observed) degree	2θ(calculated) degree	2θ difference	h	k	l
1	22.0875	22.0962	-0.0087	0	0	1
2	31.5556	31.5483	0.0073	0	2	0
3	38.7717	38.7849	-0.0132	-2	0	1
4	45.2455	45.2171	0.0284	-2	2	0
5	50.8698	50.8322	0.0376	1	1	2
6	56.1676	56.1725	-0.0049	1	3	1
7	65.8144	65.8465	-0.0321	2	2	2
8	70.4006	70.4061	-0.0055	0	4	1
9	74.9078	74.9054	0.0024	3	3	1

The broadening in the X-ray line profile is mainly due to crystallite size and anisotropic strain. Since both the effects are independent of each other we can separate out by Williamson–Hall method.

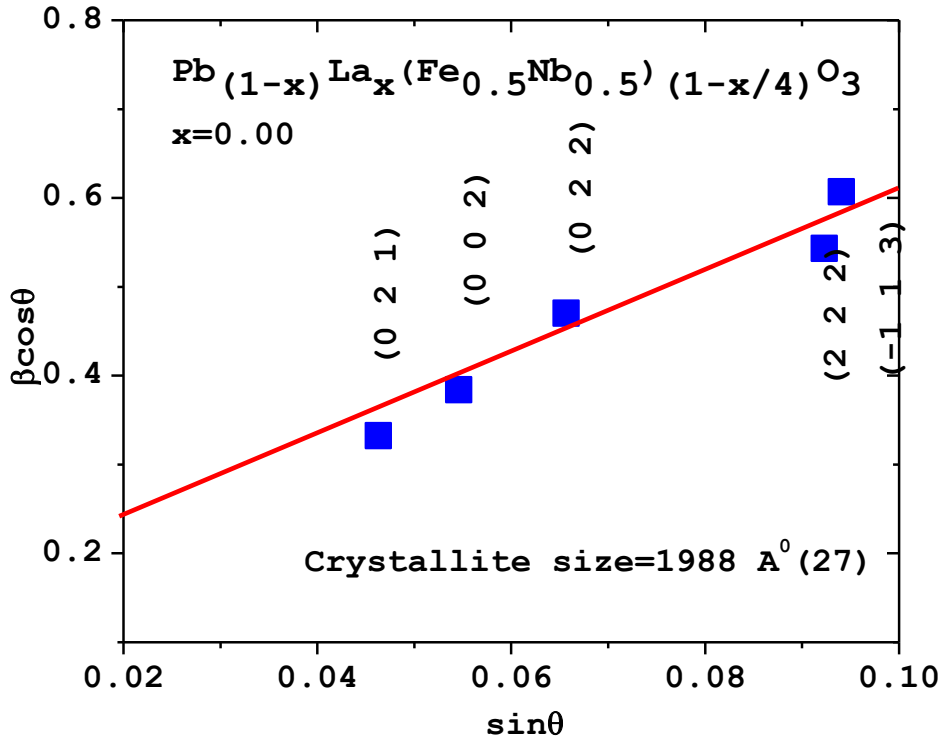

(Figure 4.1(A): Williamson–Hall plot of PFN)

Williamson-Hall equation

$$\beta \cos\theta = 4\epsilon \sin\theta + \lambda/D$$

Here, D crystallite size, λ wavelength used Є r.m.s strain in the samples.

By plotting βcos θ vs. sinθ, r. m. s. strain can be calculated from the slope and the crystallite size can calculated from the ordinate intercept. The deviation from the linear correlation corresponds to strain anisotropy. Crystallite size decreases with increase in La incorporation at Pb site of PFN.

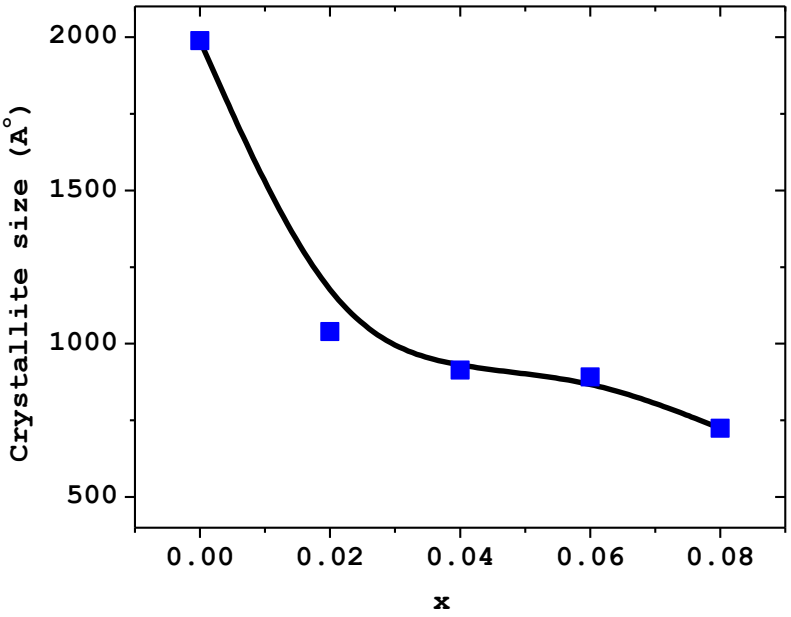

(Figure 4.1(B): Crystallite size dependence on x)

Table-4.1(f): Lattice parameters of the sample forx=0.00, 0.02, 0.04, 0.06, 0.08

Composition (x)	a(A°)	b(A°)	c(A°)	α=γ	β (degree)	Crystallite size (A°)
0.00	5.6805(44)	5.6800(47)	4.0157(09)	90	90.14	1988
0.02	5.6764(20)	5.6704(30)	4.0206(15)	90	90.13	1039
0.04	5.6764(63)	5.6712(29)	4.0163(22)	90	90.11	914
0.06	5.6754(84)	5.6700(27)	4.0179(63)	90	90.02	891
0.08	5.6721(33)	5.6716(17)	4.0228(23)	90	90.20	724

4.2 Scanning Electron Microscopy (SEM)

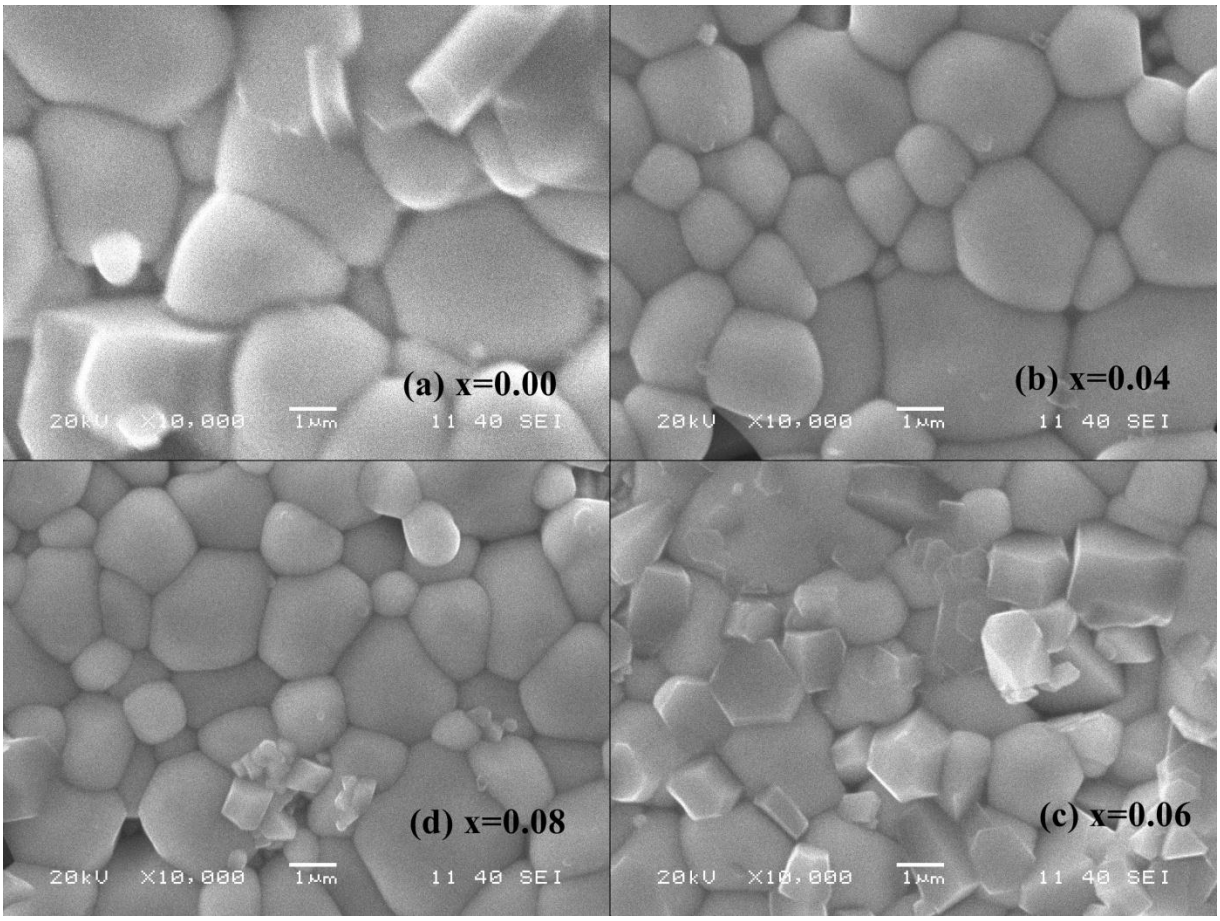

(Figure 4.2: Room temperature SEM micrographs of $Pb_{(1-x)}La_x(Fe_{0.5}Nb_{0.5})_{(1-x/4)}O_3$ (x=0.00 (a), 0.04 (b) ,0.06 (c), 0.08 (d))

The SEM micrographs show the polycrystalline nature of microstructure where grain sizes are inhomogeneously distributed throughout the sample surface with certain degree of porosity. The grain and grain boundaries are clearly distinct in the micrograph. The average grain size decreases with increase in La concentration at Pb site as observed by visual examination. The average grain size distributions of the samples were found to be 7μm to 3μm. The densification increases continuously during sintering from x=0.00 to 0.06.

4.3 Dielectric Study

Figure 4.3(a) Shows the temperature dependence of dielectric constant for La modified PFN ceramics from room temperature to 250^{o}C at several frequencies with oscillation amplitude of 1V. It is observed that $\boldsymbol{\varepsilon_r}$ decreases monotonically on increasing frequency at all the temperatures, which represents the behavior of polar dielectric materials. It can be seen from the graph that ε_r increases with increase in temperature, attains its maximum value (ε_{max}) and then decreases. As the La concentration increases from x=0.00 to 0.02, it is observed that dielectric anomaly shifts toward lower temperature and falls below the room temperature for x=0.04, 0.06, 0.08. This dielectric anomaly is observed for La-modified PFN represents the ferroelectric – paraelectric phase transition which is diffuse type. It is also observed that dielectric constant decreases with increase in La substitution at Pb site which may be due to switching off of polarizibility of Pb in PFN. The former observation is related to the decrease of grain size due to the La^{3+} ions doping as observed from SEM and also decrease in crystallite size as seen from XRD. **Figure 4.3(b)** represents the temperature dependence of tanδ for selected frequencies. It is observed that for all the samples tanδ increases on increasing temperature with one anomaly in the temperature range 50-250^{o}C .This anomaly in tanδ shifting towards the high temperature side and the broadening of the peak increases with increase in frequency. The reason for increase in tanδ at high temperature is due to the generation of space charge polarization in the ceramic materials. Rapid increase in tanδ at high temperatures is attributed to increase in electrical conductivity of the material.

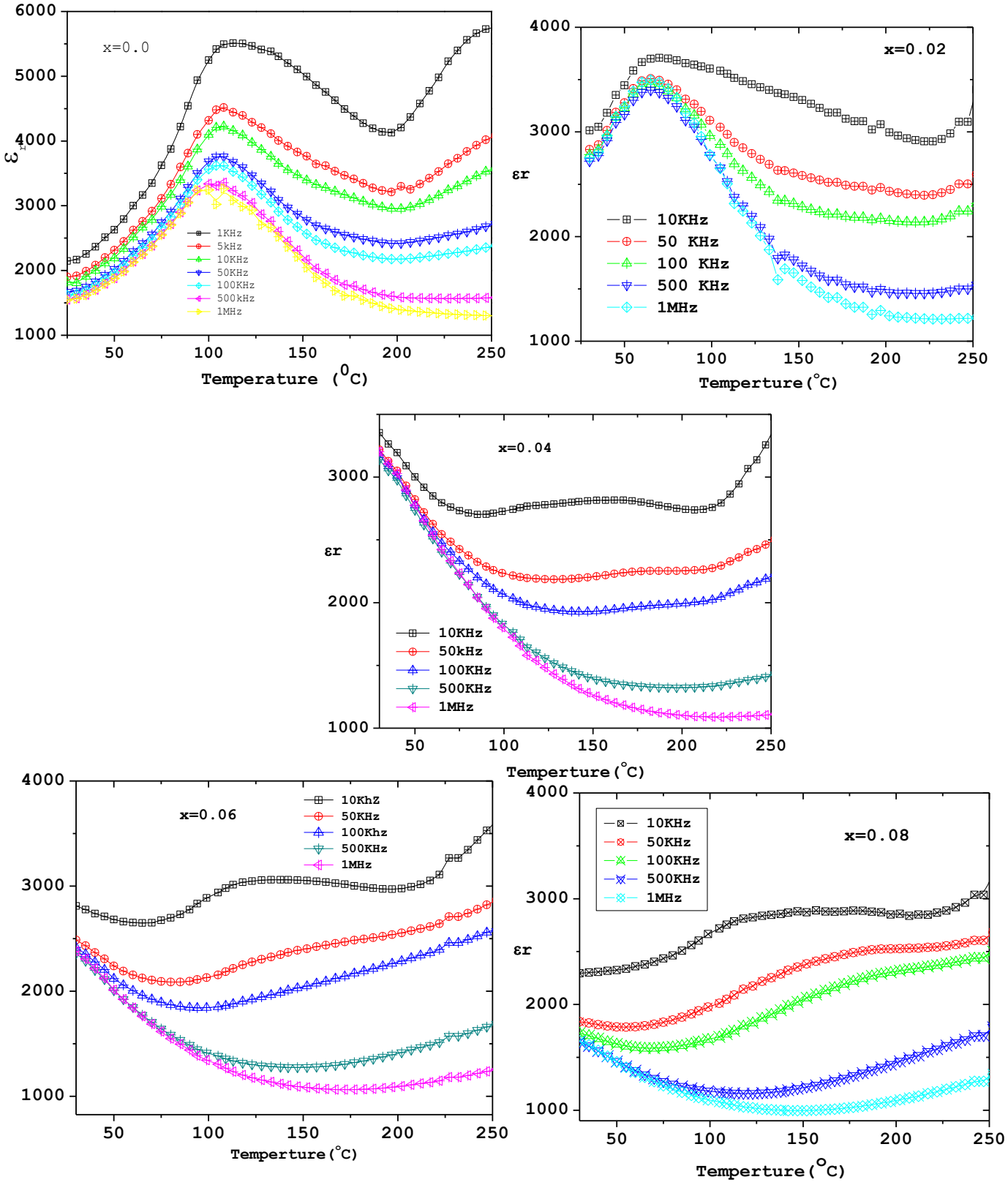

(Figure 4.3(a): Temperature dependence of dielectric constant for $Pb_{(1-x)}La_x(Fe_{0.5}Nb_{0.5})_{(1-x/4)}O_3$ (x=0.00,0.02,0.04,0.06,0.08))

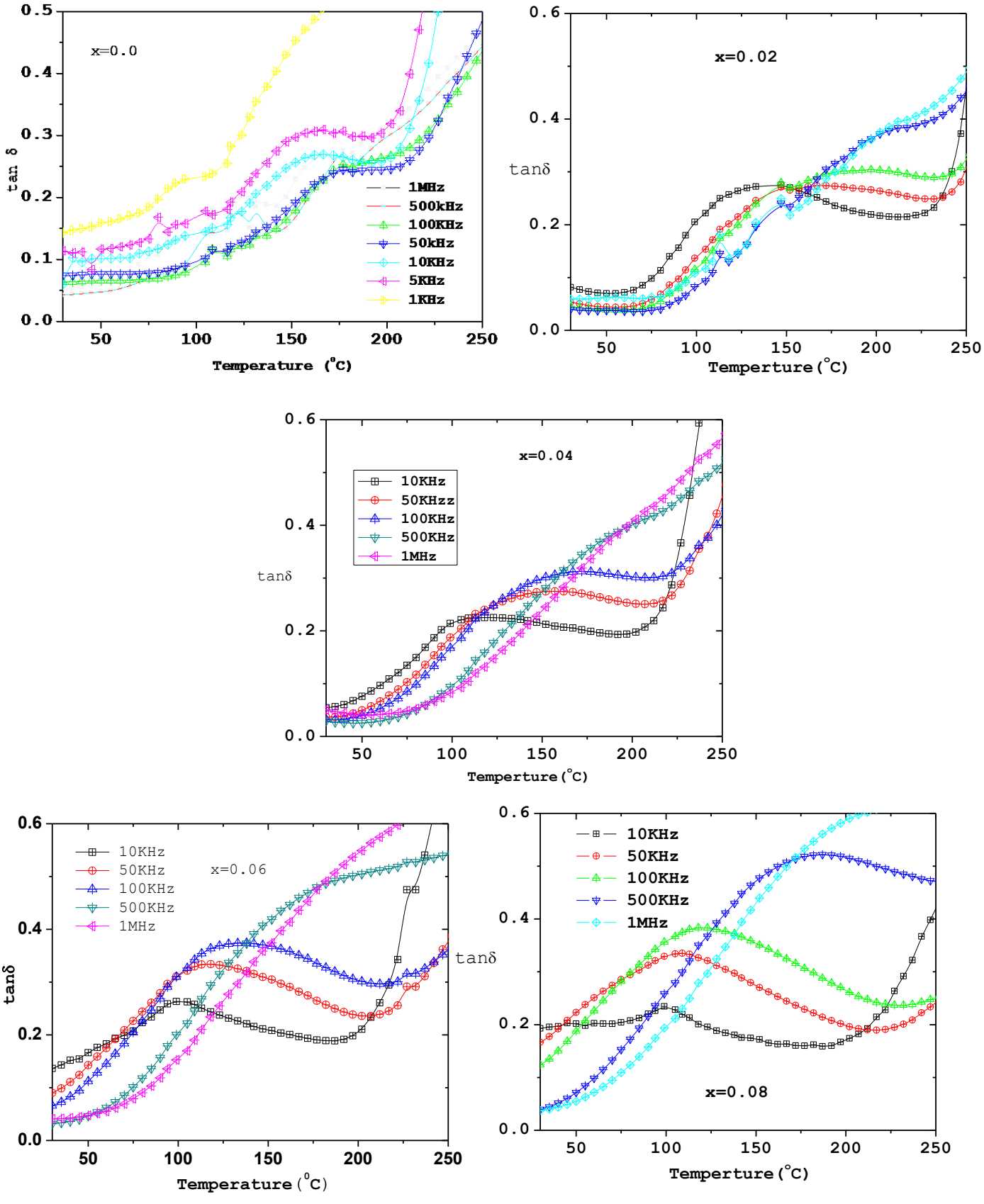

(Figure 4.3(b): Temperature dependence of dielectric loss (tanδ) for $Pb_{(1-x)}La_x(Fe_{0.5}Nb_{0.5})_{(1-x/4)}O_3$ (x=0.00, 0.02, 0.04, 0.06, 0.08))

4.4 Conductivity studies

Figure 4.4 Shows the variation of ac electrical conductivity (σ_{ac}) of PFN as a function of frequency at different temperatures and for all La modified PFN ceramics. The a.c. conductivity was calculated using the relation $\sigma_{ac} = \varepsilon_o\varepsilon_r\omega \tan \delta$. In the low frequency region, ac conductivity remains frequency independent, representing d.c conductivity. Whereas the dispersion of conductivity was observed in the higher frequency region. The crossover from the frequency independent region to the frequency dependent regions represents the starting of the conductivity relaxation, indicating the transition from long range hopping to the short-range ionic motion in the compound. The frequency dependence of ac conductivity obeys Jonscher's power law, i.e. $\sigma_{ac} = \sigma_0 + A\omega^n$, where σ_0 is frequency independent conductivity (which is related to dc conductivity), A is the temperature dependent pre-exponential factor and n is frequency exponent, $(0 < n < 1)$. As ac conductivity increases with rise in temperature, all the compounds have negative temperature coefficient of resistance (NTCR) behavior which is the typical behaviour of semiconducting material.

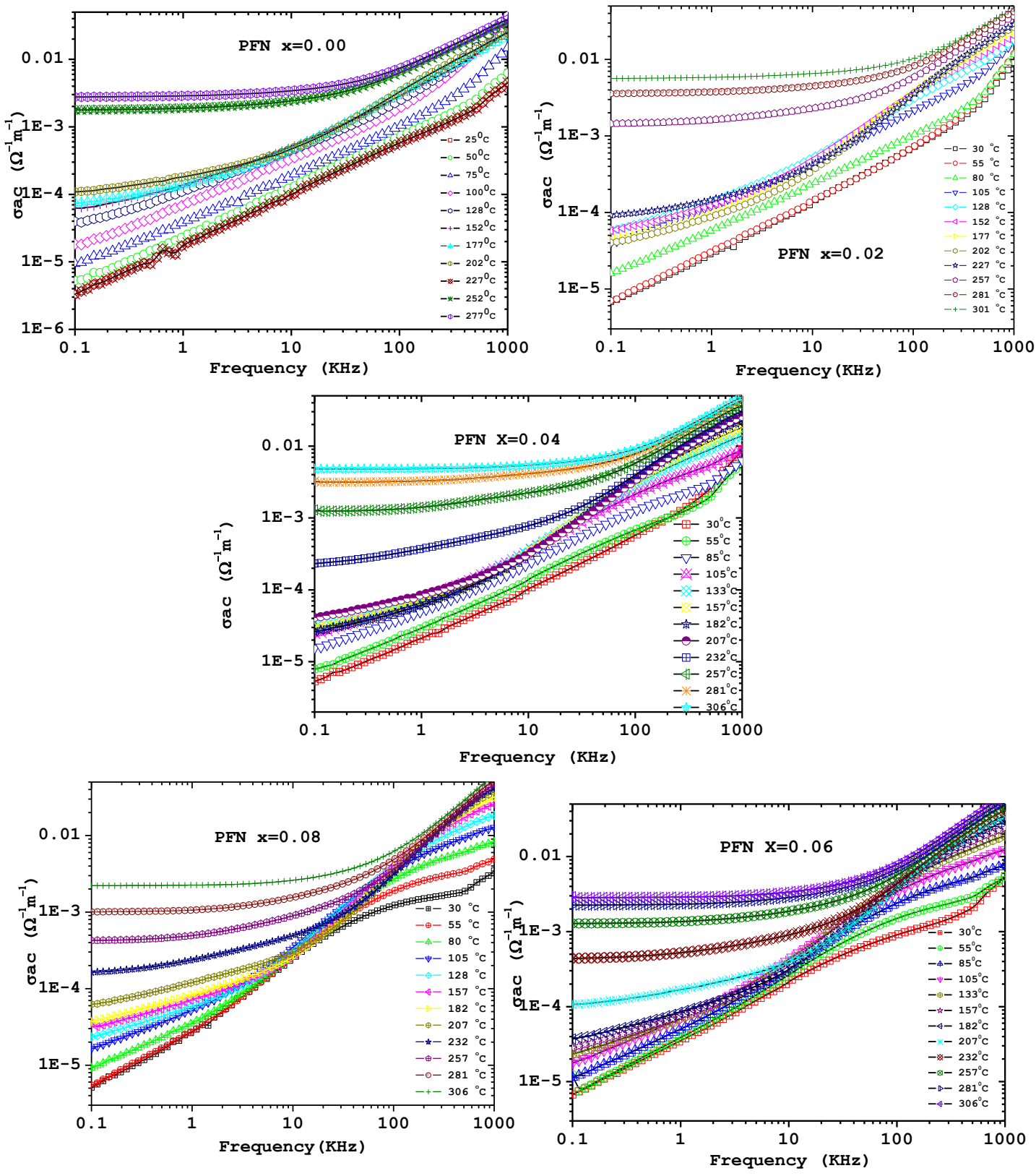

(Figure 4.4: Frequency variation of σ_{ac} for $Pb_{(1-x)}La_x(Fe_{0.5}Nb_{0.5})_{(1-x/4)}O_3$ (x=0.00, 0.02, 0.04, 0.06, 0.08))

4.5 Impedance Spectroscopic studies

Figure 4.5 represents the temperature dependent complex impedance (Nyquist plot) of La-modified PFN ceramics. The linear variation of $Z^{//}$ with $Z^{/}$ in the complex impedance plot in low temperature range from room temperature to 200°C indicates the insulating properties of the material. Above 200 °C, circular arc formation trend started which is due to the increase of conductivity. The impedance plots seem to have two overlapped semicircles. Each semicircle of the Nyquist plot corresponds to the different contribution to the electrical response. The high frequency semicircle can be attributed to the bulk (grain) property and low frequency corresponds to grain boundary property of the material .The relaxation process is non-ideal or non-Debye type in nature. The intercept of the semicircular arc on the real axis of the complex impedance plane gives the dc resistance of the material. It is seen that the dc resistance increases with increase in the Lanthanum concentration in the material.

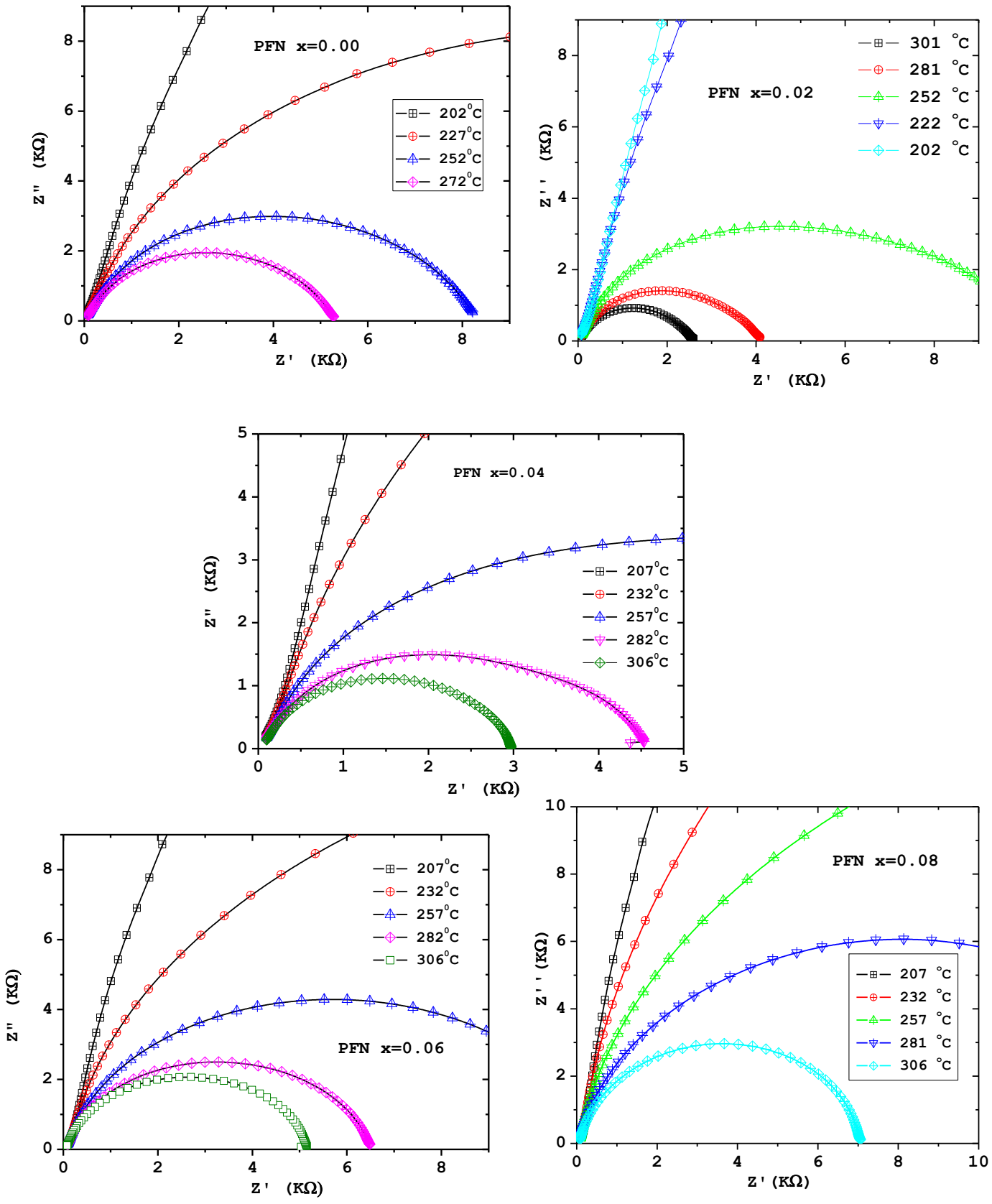

(Figure4.5: Nyquist plot for $Pb_{(1-x)}La_x(Fe_{0.5}Nb_{0.5})_{(1-x/4)}O_3$ (x=0.00, 0.02, 0.04, 0.06, 0.08))

CHAPTER 5

Conclusion

In the present work, we have synthesized and studied the complex perovskite ceramics oxides having the general chemical formula $Pb_{(1-x)}La_x(Fe_{0.5}\ Nb_{\ 0.5})_{(1-x/4)}O_3$ (x=0.00, 0.02, 0.04, 0.06, 0.08). The structural (XRD), microstructural/morphological (SEM) and electrical (dielectric and impedance) properties of the proposed compounds have been studied extensively.

Based on our results following conclusions have been made.

- PFN and La-modified PFN samples were prepared by high temperature solid-state reaction route
- X-ray diffraction (XRD) studies show the formation of the compounds with monoclinic crystal system. Lattice parameters and crystallite size obtained from XRD data found to be decreased with increase in La^{+3} concentrations.
- Scanning electron micrographs of the compounds showed (1) polycrystalline nature of microstructure, (2) decrease in grain size with increase in La^{+3} concentration, (3) uniform distribution of grain size with high density.
- The ferroelectric phase transition temperature was found to be 115^oC for PFN and decreases with increase in La^{+3} incorporation and falls below the room temperature for x=0.04, 0.06 and 0.08.
- The ac conductivity of the La-modified PFN obeyed the Jonsher's power law behavior.
- Complex impedance spectroscopy method has been employed for better understanding of relaxation process and to establish relationship between the microstructure–electrical properties of the compounds.

References

1. G Haertling. *Journal of American ceramic Society* 82, 797 (1999).
2. Jona & Shirane, Ferroelectric crystals, over publication New York.
3. C. B. Carter and M. G. N. Norton, Ceramic materials, Springer.
4. Kittel, Introduction to solid state physics, WILEY publication.
5. Zuo-Guang Ye, Handbook of advanced dielectric, piezoelectric and ferroelectric materials, Woodhead pub. Ltd. And CRC Press LLC, 2008.
6. G. A. Smolenskii and V. A. Bokov, J. Appl. Phys. 35,915 (1964)
7. Raymond et al. *Journal of Applied Phys.* 97, 084108(2005).
8. Wang et al. *Applied Physics Letters* 86, 192507(2005).
9. Kumar et al. *Applied Physics Letters* 60(1992).
10. Mishra et al. *Journal of physics. Condensed matter* 22(2010).
11. Sahoo et al. *Physica B*, 406(2011).
12. R.R. Vedantam et al. / Materials Science and Engineering B 113 (2004).
13. A.J. Moulson and J.M. Herbert, Electroceramics, WILEY publication.
14. S Ananta, N. W. Thomas, Journal of the European Ceramic Society 19 (1999).
15. B. D. Cullity, X-ray diffraction, Addison-Wesley Pub, 1978.
16. P. J. Goodhew, J. Humphreys, R. Beanland, Electron Micriscopy and analysis, Taylor & Francis, 2001.
17. Singh et al. *Applied Physics Letters* 90,242915 (2007).
18. Cohen et al. *Physical Review B*, 42, (1990).
19. S.-B. Lee et al. / journal of the European Ceramic society 24 (2004).
20. J. R. MacDonald, Impedance Spectroscopy, Wiley, New York, NY, USA, 1987.